RESULTS OF ATOM INTERFEROMETRY EXPERIMENTS WITH POTASSIUM

John F. Clauser

Department of Physics
University of California, Berkeley
Berkeley, California 94720

Results of high flux atom interferometry experiments with potassium in generalized Talbot-Lou configurations are presented. The interferometer consists of a sequence of three planar vacuum-slit diffraction gratings, microfabricated from silicon nitride membranes. Interference fringes are sensed by measuring the transmission of atoms on a hot-wire as a function of grating relative position. Different spatial Fourier components in the diffraction pattern are resonant in the interferometer at different atomic velocities. When a laser cooled slow beam is incident, various different diffraction patterns are observed as a function of atomic velocity, selected via the tuning of cooling lasers. In an alternative "Heisenberg Microscope" configuration an incident thermal beam produces a velocity average over different fringe patterns that averages over and washes out the high frequency Fourier components. In this configuration AC modulated laser light passes through the interferometer. Via the Doppler shift, it is scattered only by atoms in a narrow velocity band. Since imaging of the fluorescent light *could* determine which slit an atom passes, the laser destroys, and thereby reveals via the AC modulation, the associated high-frequency fringe contribution.

Key words: atom, interferometer, matter wave, de Broglie wave.

1. INTRODUCTION

Following suggestions by Altshuler and Frantz [1], Dubetskii *et al* [2], and Clauser [3], there is recent interest in experimentally demonstrating de Broglie wave interference exhibited by the propagation of whole neutral atoms [4–8]. Atom interferometry experiments, in essence, are striking de Broglie-wave variants of Young's two-slit experiment. The experiments

M. Ferrero and A. van der Merwe (eds.), Fundamental Problems in Quantum Physics, 57–71.

described here are a N-slit extension of this. Given my own earlier experimental and theoretical work on Bell's theorem [9], I do not agree with R. Feynmann's assertion that the two-slit experiment contains the *whole* mystery of quantum mechanics, but I do agree that it embodies a big chunk of it!

An atom such as potassium is a very complicated thing. It contains electrons, virtual photons and a nucleus, further comprised of nucleons and mesons, in turn full of quarks, gluons, and lots of virtual stuff, much of which we probably have not yet conceived. How do big whole atoms exhibit spatial de Broglie wave interference? The Hamiltonian for such a beast is a sum over the kinetic and internal potential energies of the atom's constituent parts. By the *magic* of the center-of-mass transformation, this sum can be split into a sum of two parts [10]. The first part is the Hamiltonian studied by spectroscopists. The second part represents the kinetic energy of a moving point particle, whose mass is that of the whole atom. Atom interferometry experiments exploit the latter part, and/or both parts. Yet despite an atom's hopelessly complicated composite structure, it remains undisturbed as a whole atom, even after it passes simultaneously through more than one slit at a time. How does it do so? Beats me!

2. INTERFEROMETRY USING A COLD SLOW ATOM SOURCE

This paper summarizes the results of two different experiments demonstrating atom spatial interference. See Refs. 4 for more details. The apparatus for the first experiment is diagramed in Fig. 1. Two copropagating potassium beams pass simultaneously through an atom interferometer and are detected by surface ionization on a hotwire [11]. The first is temporally continuous (DC), and has a thermal velocity distribution broadly peaked at about 540 m/sec. It acts as a "parent" for the second beam. The second beam is temporarily chopped (AC) and synchronously detected to allow it to be distinguished it from the first. The AC beam is slow ($v \approx 182$ m/sec) and cold. Figure 2a shows two possible computer simulated velocity profiles for the slow beam. Due to peculiarities of the cold beam's production and detection methodology, its velocity profile has phase-reversed wings. The DC thermal beam is produced by scattering near the oven's exit slit, which is displaced from the interferometer's axis. It is about 130 times more intense than the slow beam. The latter is velocity selected by using AC modulated (chopped ON and OFF at 6 Hz) laser light, incident on the thermal beam at 20°. Scattering of about 7 photons by each slow atom deflects it out of the low velocity portion of the parent beam's thermal distribution, onto the interferometer's axis. The parallel component of the laser's incidence provides

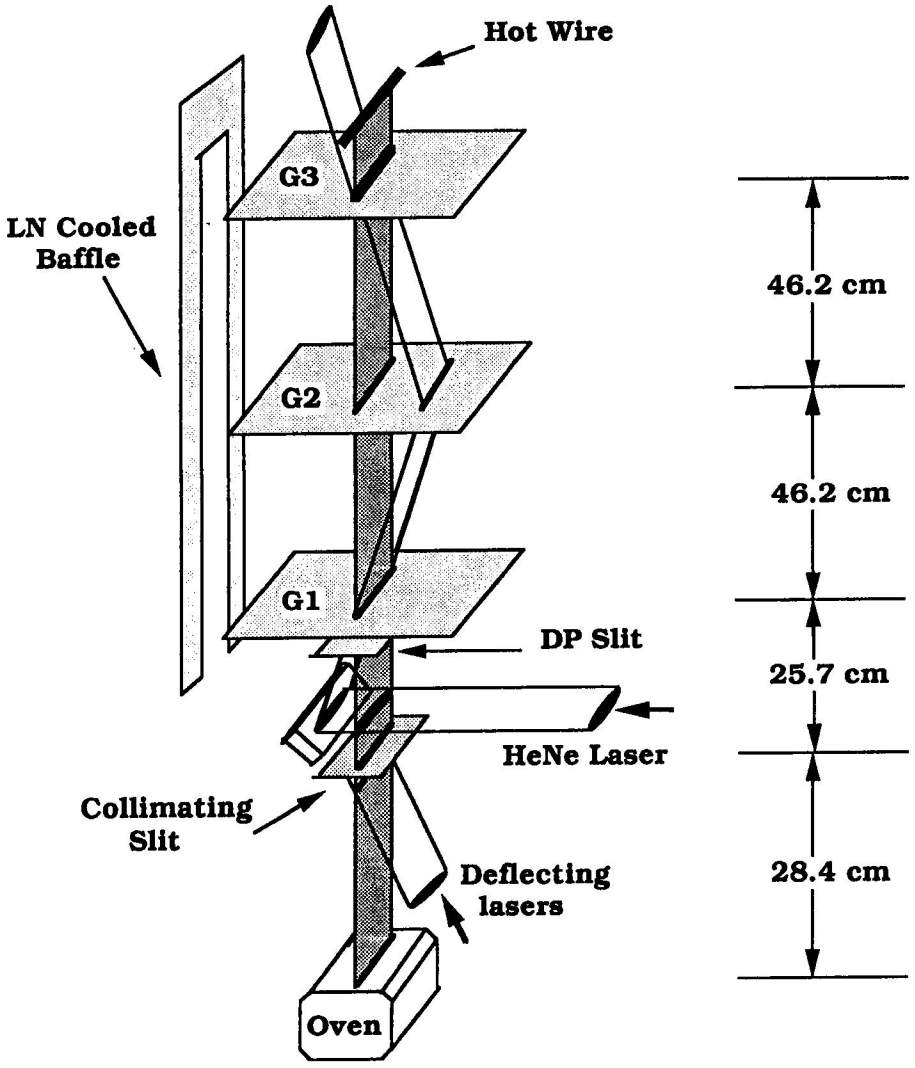

Fig. 1. Geometry of the experimental apparatus used for experiments with a cold slow incident atomic beam. A HeNe laser beam passing through the gratings is used for rotational alignment of the interferometer.

Doppler velocity selection, while the perpendicular component provides momentum transfer for deflection.

Typical lateral spatial profiles of the slow (AC) and thermal (DC) beams are shown in Fig. 3. Perpendicular heating of the slow beam by random recoil of fluorescent photons, predicted by Einstein [12] and sought experimentally by Frisch (unsuccessfully, without the benefit of laser tech-

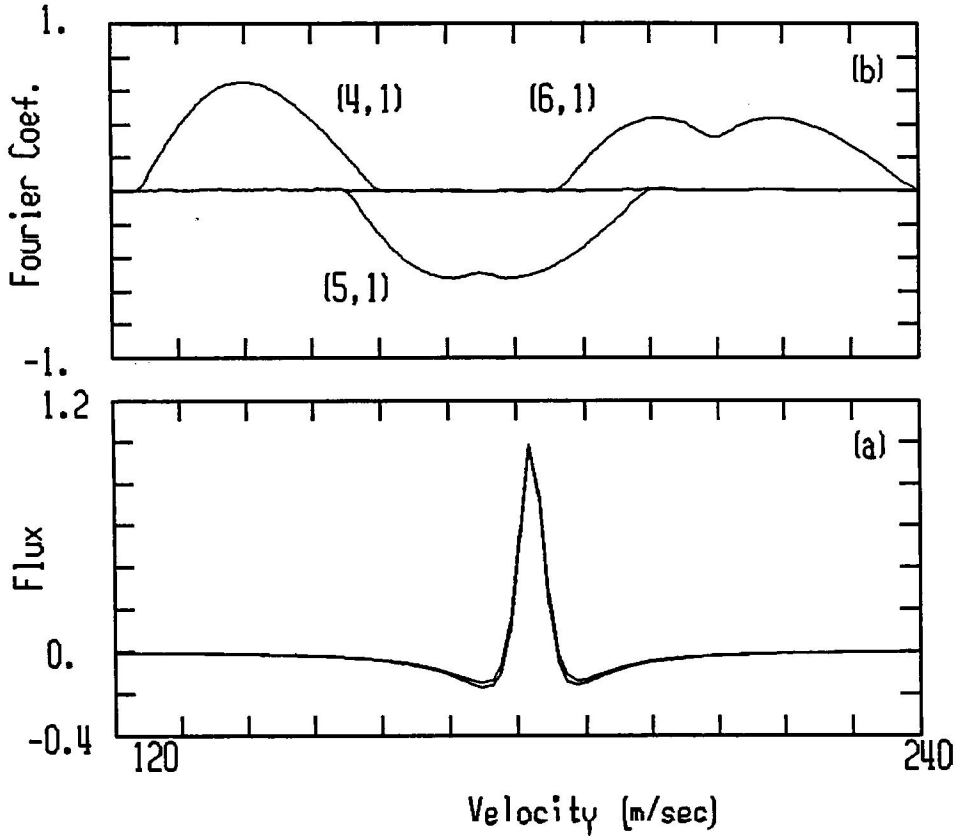

Fig. 2. (a) Two possible velocity profiles for our source, assuming a parallel velocity spread of about 10–12 m/sec. Positive and negative signs correspond to in-phase and phase-reveresed AC signal levels. (b) 4th, 5th, and 6th spatial harmonic content of the calculated fringe pattern at the respective (m,n) = (4,1), (5,1) and (6,1) resonances.

nology) [13], is evident in the data. The effective source brightness for cold slow (182 m/sec) atoms is about 4×10^{15} atoms $\mathrm{cm}^{-2}\mathrm{sr}^{-1}\mathrm{sec}^{-1}$, yielding a maximum transmitted and detected current of roughly 4×10^5 atoms per sec.

The interferometer consists of a sequence of three parallel planes, each containing a rectangular vacuum-slit transmission grating, G_1, G_2, and G_3, respectively. The spacings between the grating planes are $R_1 = R_2 =$ 46.2cm. The gratings are micro-fabricated from 1μ thick silicon-nitride membranes supported by silicon frames, with parallel slits etched through the membranes. Gratings G_1 and G_3 have the same period, $a_1 = a_3 = 16.2\mu$, and have 22 and 75 slits, respectively. Grating G_2 has 111 slits, with a period, $a_2 = 8.1\mu$. All three are 8.5 mm long and have an average open fraction

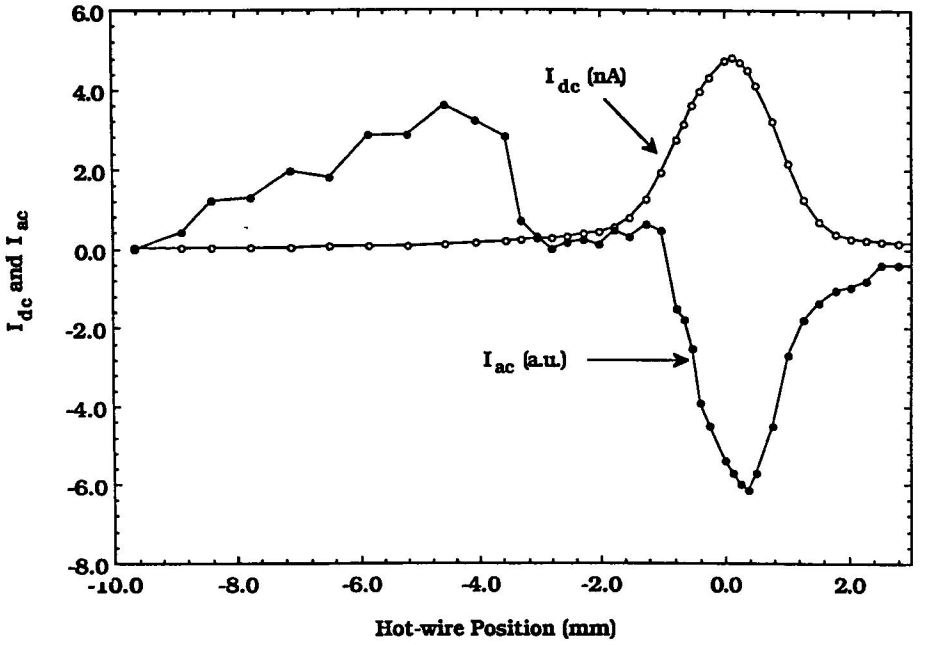

Fig. 3. Spatial profiles of the DC parent thermal beam and AC chopped cold slow beam by scanning the position of the hot-wire detector. These profiles were taken at a laser tuning to select atoms at 295 m/sec, with high laser power, and with no intervening interferometer. For the first interferometry experiment the oven's position is offset so that the deflected AC beam is along the interferometer axis.

of about $s/a = 1/8$, where s is the slit width.

For an interferometer with the above geometry Clauser and Reinsch pointed out that de Brolige-wave fringes will be formed on and masked by G_3 via the generalized Talbot-Lau effect [14]. Fringes are sensed by monitoring the variation of the transmission in response to slowly scanning G_2's position. An interfering path set within the beam envelope consists of nested diamonds, starting at one source slit of G_1, and forming an interference pattern on G_3. Solid-angle acceptance is enhanced (by a factor of almost 10^7 over the atom interferometer geometry used by Keith *et al.* [7]) by incoherent addition of the current from many source slits on G_1, each providing many such nested diamonds at all possible skew angles between the slits of G_1 and G_2.

With low velocity monochromatic illumination an interference pattern is thus formed. The fringe pattern (and the transmitted current) contains various spatial harmonics of the geometric shadow Moiré period. Each harmonic will be resonant in the interferometer at a different atomic ve-

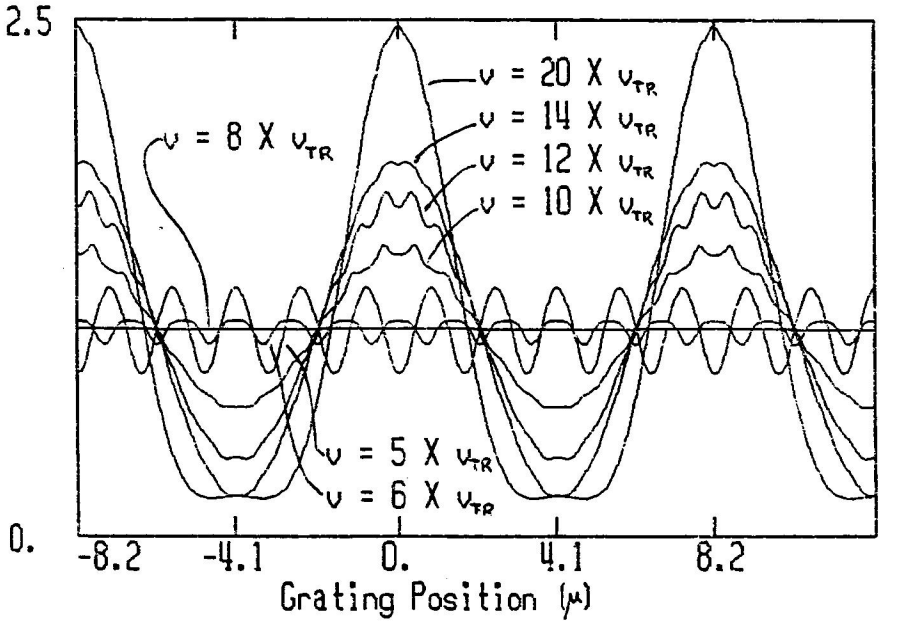

Fig. 4. Calculated normalized interferometer transmission as a function of and grating displacement, for various atomic velocities, 175, 210, 280, 350, 419, 489, and 699 m/sec, corresponding to 5, 6, 8, 10, 12, 14, and 20 times v_{TR}, respectively.

locity. Figure 2b shows the calculated amplitudes for the 4th, 5th and 6th harmonic components of a Fourier decomposition of the pattern as a function of atomic velocity. A resonance for the m'th harmonic occurs at $\lambda_{dB}/\lambda_{TR} = n/m$ when m and n approximate small integers. Here, λ_{dB} is the atoms' de Broglie wavelength, $\lambda_{TR} \equiv a_2^2/\rho$ is the interferometer's Talbot-Rayleigh wavelength, and $\rho \equiv R_1 R_2/(R_1+R_2)$ is the interferometer's reduced length. For our geometry the associated resonant atomic velocity is $m/n \times V_{TR}$, where $V_{TR} \approx 35$ m/sec. Phase reversal of the $(m,n) = (5,1)$ resonance (5th harmonic) is a consequence of the fact that the product, $m \times n$, is odd.

Figure 4 shows for various atomic velocities the calculated interferometer transmission as a function of G_2 displacement, averaged over the finite slit widths G_1 and G_3. At velocities above $a_2/s_2 \times v_{TR} \approx 8\ v_{TR} =$ 278 m/sec, the oscillatory fringe structures give way to the $(n \rightarrow 0)$ geometric shadow Moiré. The calculated AC and DC signals at any grating position are given by a weighted integration of the transmission over atomic velocity. For the AC signal, a weighting by the velocity profile of Fig. 2a samples a narrow range of the velocities where high frequency oscillatory fringe structures occur. A thermally distributed weighting washes out the

high-frequency structures and yields a diffraction limited geometric Moiré for the DC fringe pattern.

Figure 5a shows the measured (solid) and calculated (dashed) DC signal as a function of grating position, while Fig. 5b shows the simultaneously measured AC signal in response to a single scan of G_2's position. Each data point represents about a 4 sec integration. Due to a start-up hysteresis in our piezoelectric translator, the G_2 displacement axis suffers from a nonlinear distortion for negative values, evident in both the AC and DC signals. Despite this distortion a fifth spatial-harmonic component is evident in the AC signal. Since the laser tuning selects atoms near the $(m,n) = (5,1)$ resonance, this harmonic is expected to dominate. However, given the v^3 weighting of atoms in the parent beam, the phase-reversed high-velocity broad Lorentzian wing of the profile contributes significant sixth harmonic at opposite phase that enhances end fringes and washes out central fringes. Figure 5b also shows the associated calculated AC fringe patterns for the two assumed incident AC velocity profiles of Fig. 2a.

Since the interferometer is highly velocity selective, a small change in the excitation spectrum has a strong effect on the shape of the pattern. Had we instead assumed a broad non-reversed velocity profile in our simulation, the strong peaks would be shifted by half a DC fringe period. It also has a significant effect on the vertical offset of the pattern (suppressed in Fig. 5b), since the 5th and 6th (modest visibility) harmonics have opposite phase. Cancellation of the associated opposite vertical offsets enhances the apparent AC fringe visibility. Thus, although the observed AC fringe visibility is about 80% referenced to the blocked-laser AC signal level, that of each velocity component is probably lower. Calculation assuming various s/a values indicates that the asymmetry and finite visibility of the DC fringe pattern are due dominantly to quantum-mechanical diffraction by G_2 and more weakly to geometrical averaging by G_1 and G_3.

3. "HEISENBERG MICROSCOPE" DECOHERENCE ATOM INTERFEROMETRY

Recently, Walls *et al.* [15] analyzed a problem, analogous to that of the "Heisenberg microscope," for freely propagating atoms with well defined momenta that form de Broglie-wave fringes in a Young's two-slit interferometer. They consider a situation wherein both slits are simultaneously illuminated with light that is resonant with an atomic transition, and calculate the resulting atomic fringe visibility as a function of slit separation. They predict that when the slits are separated sufficiently, so that a Heisenberg microscope viewing the reemitted fluorescence can image this light to determine which slit an atom passes, then the atomic fringe visibility will vanish.

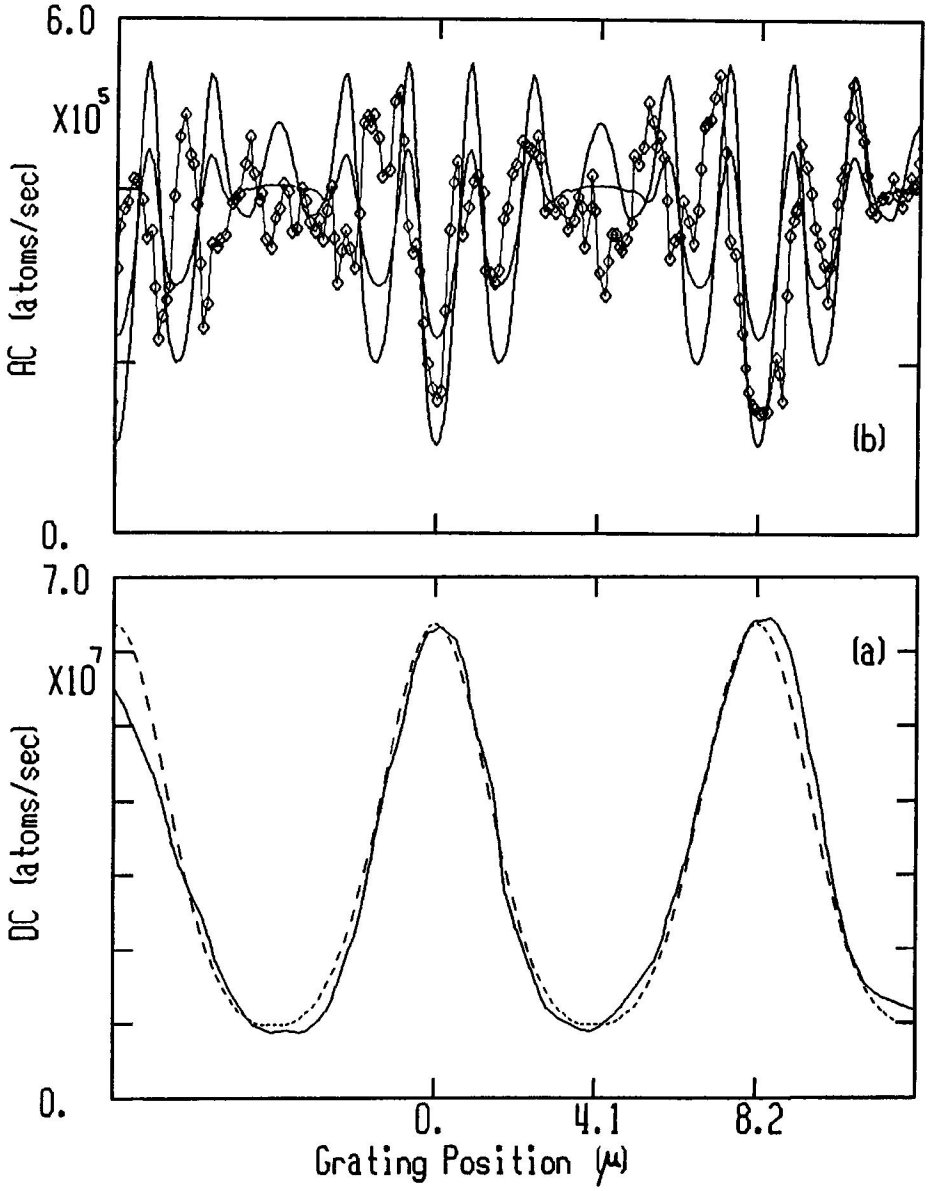

Fig. 5. (a) Measured (solid line) and calculated (dashed line) DC signal as a function of grating relative displacement. Zero level corresponds to the laser-blocked condition. (b) Simultaneously measured AC signal (diamond points) and calculated AC signals (with the vertical offsets suppressed), for the different assumed velocity distributions of Fig. 2a.

But when the slit spacing is comparable to the optical wavelength, such a

determination by the microscope exceeds its resolving power, and then the interference pattern will persist. Further, the presence of the microscope is unnecessary for the predicted visibility dependence on slit spacing to obtain (none is present in our experiment). Only the microscope's illumination need be present.

The above predictions can be tested. Indeed, Sterr *et al.* [8] destroyed atom interference fringes by passing high intensity resonant laser light through their atom interferometer. In that experiment many photons were scattered off of each atom, and while their atomic paths have an amplitude for being physically separated in space, actually the paths are continuously distributed in space and are not clearly localized by a scattering event. In our experiment we destroy atom interference fringes by the scattering of a single low energy photon by an atom. Thus, with no microscope illumination (and no scattering) amplitudes for an atom's passage simultaneously through more than one physically different slit provide quantum interference and produce a multiple slit interference pattern. With illumination, however, a scattering can localize an atom's path to a region smaller than the slit spacing. Given the multiply connected geometry an atom, thus localized, can pass through only one slit. Hence the scattering can be used to determine which slit the atom passes, whereupon no fringe pattern will form.

The above process is used by our second atom interferometry experiment. A high spatial frequency interference fringe pattern is revealed by its destruction. Now only a thermal potassium beam is transmitted through the same velocity selective atom interferometer used above. Atoms at characteristic resonant atomic velocities (and/or de Broglie wavelengths) form fringe patterns that contain high spatial-frequency Fourier components. As indicated in Fig. 5a, the thermal velocity distribution produces an average over these components that washes out and hides the high frequency fringes. AC modulated laser light now passes through the interferometer near G_2. Since imaging of the fluorescent light *could* be used to determine which G_2 slit an atom passes, the contribution to the averaged pattern by atoms at the laser's Doppler shifted wavelength is removed. That component is thus AC modulated and detected. Potassium's hyperfine structure effectively limits the number of scatterings per atom to about one via the high probability that following a scattering the atom will optically pump and thereafter be transparent to the laser radiation [16]. To further assure only one scattering per atom in an atom's flight time through the laser beam, and to provide a narrow effective laser bandwidth, the laser is attenuated heavily.

The apparatus, shown in Fig. 6, is a modification of that of Fig. 1. The oven is now located on the axis and the deflecting laser light is not used. Instead, "microscope illumination" consists of a highly attenuated AC chopped laser beam passing through the interferometer at near anti-

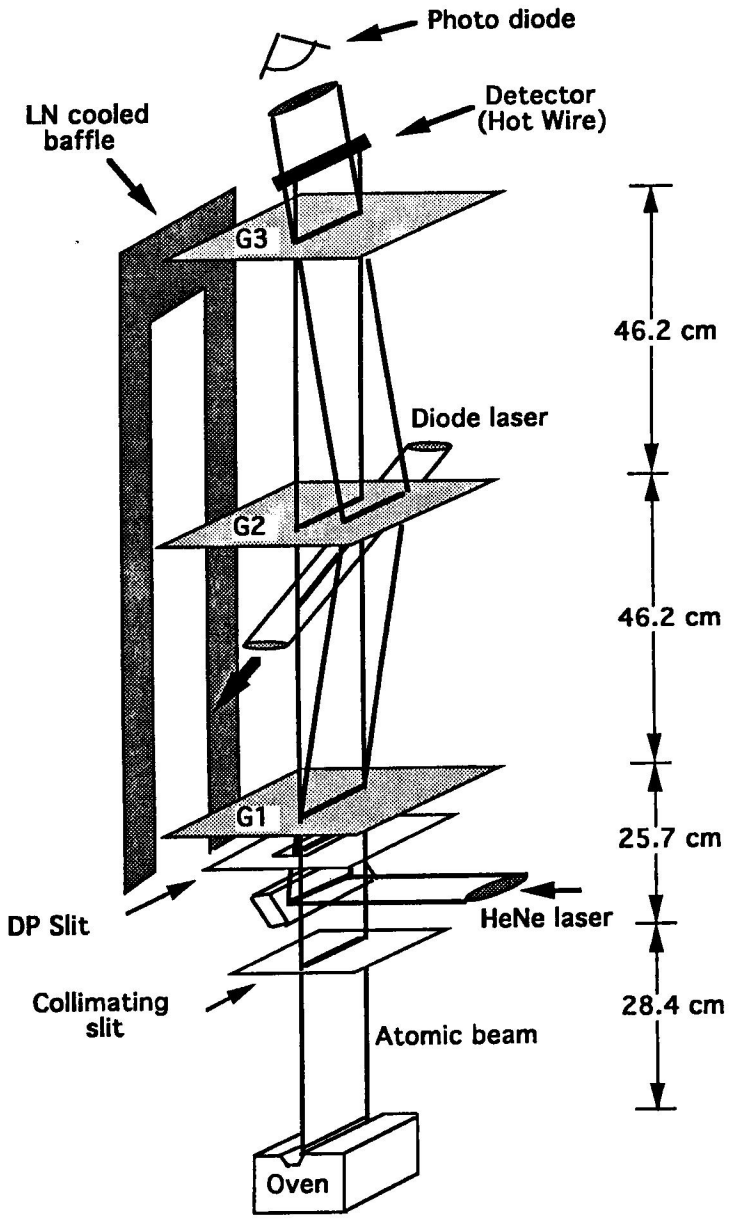

Fig. 6. Geometry of the experimental apparatus for the Heisenberg microscope experiments. The photomultiplier used to measure fluorescence intensity is not shown.

parallel incidence (20°) to the beam, immediately below G_2. When the laser is (OFF), then interference fringes are formed, but the beam's thermal

velocity average prevents their direct observation. When the laser is ON, it resonates with two different velocity groupings of atoms, since K^{39} has two atomic ground-state hyperfine levels ($F = 1, 2$). $F = 2$ atoms will be resonant only for tunings with $v_{F=1}$ greater than 351 m/sec, the velocity Doppler equivalent of the hyperfine resonance spacing.

We calculate the laser-ON transmission probability, assuming a kinematical scattering near G_2 of one photon by each atom, assume a classical atomic trajectory, and use the point-wise momentum-transfer photon scattering model by Einstein [12] in his discussion of the kinematics required for thermal equilibrium to obtain when a gas is irradiated by thermal light. We first consider a line source of atoms at G_1 and the scattering of one incident circularly polarized photon near G_2, and then calculate the transmission by a single G_2 slit. Summing the result over the various slits in G_1, G_2, G_3 and averaging over the associated G_1 and G_3 slit widths yields the laser-on transmission probability, given the scattering of one photon. The transmitted AC current is given by the difference between this transmission probability and that for no laser light, averaged over the thermal velocity distribution, and weighted by the probability that an atom will scatter one (and only one) photon in an atom's transit through the laser beam. This probability has two resonant near-Lorentzian components separated by 351 m/sec, corresponding to and weighted by the thermal hyperfine level populations, 40% $F = 1$ and 60% $F = 2$.

To observe interference fringes, the laser is tuned to resonate with $F = 1$ atoms at a velocity of 211 m/sec, i.e. 6 times the Talbot-Rayleigh velocity, $v_{TR} \approx 35$ m/sec, corresponding to AC fringes at the sixth spatial harmonic of the geometric shadow period. While holding the laser tuning constant, G_2 is scanned laterally, and the DC and AC signals are recorded simultaneously. These signals are shown as a function of G_2 displacement, Δx, in Figs. 7a and 7b, along with the calculated DC and AC currents. The sixth spatial harmonic associated with the Talbot-Lou resonance is evident in the AC signal's data.

To observe the velocity dependence of the AC signal, G_2's position is held fixed and the laser tuning is swept. The measured signals obtained when the gratings are positioned for minimum and maximum transmitted DC current are shown in Figs. 8a and 8b, along with the calculated signals. Agreement between the calculated and measured signals appears to be quite good.

For comparison, in Fig. 8c we show the laser excited fluorescence intensity measured using a photomultiplier and the same laser incidence angle (but with no gratings present) in response to a similar laser frequency scan. We note that the hyperfine structure is not resolved in the fluorescence spectrum. By contrast, the transmission spectrum of Fig. 8a displays two well-resolved peaks whose the spacing corresponds to the hyperfine struc-

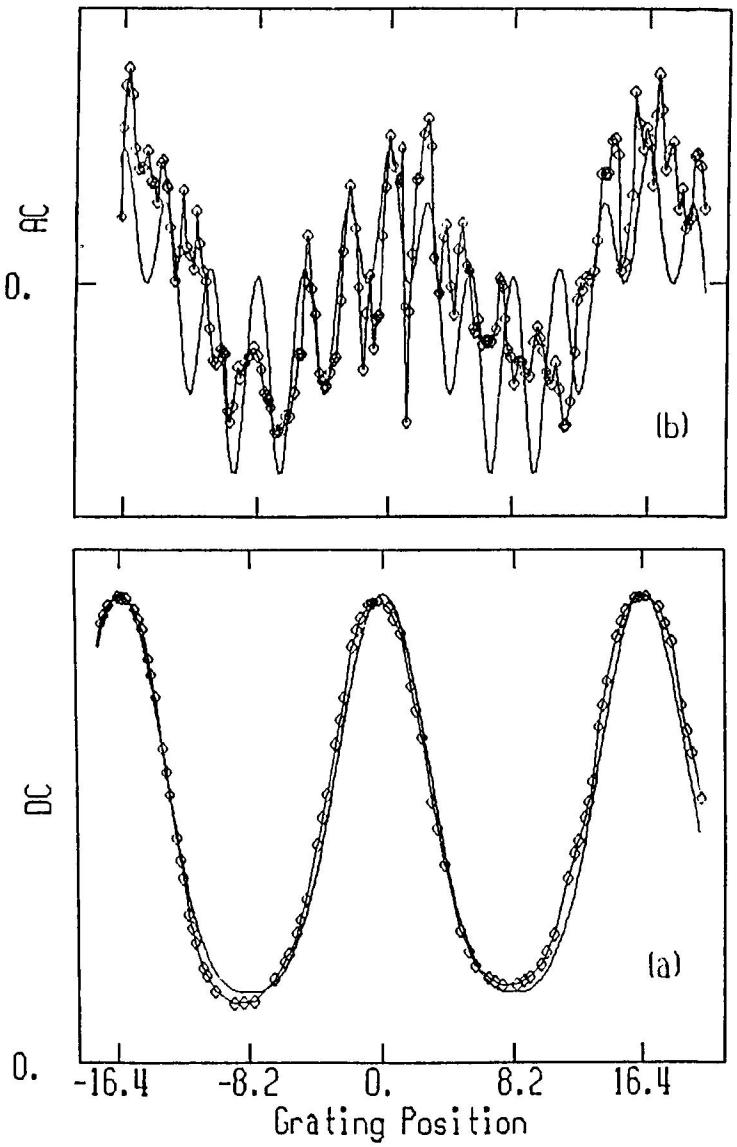

Fig. 7. Calculated and observed (diamond points) atomic currents as a function of grating relative displacement, Δx (microns). (a) DC signal due to thermal beam illumination, (b) AC signal showing the destroyed fringes for atoms at 211 m/sec. To give better agreement between the observed and calculated AC patterns, a small DC signal cross-talk component is added to the calculated AC signal.

ture. Evidently we have constructed what amounts to an atom interference

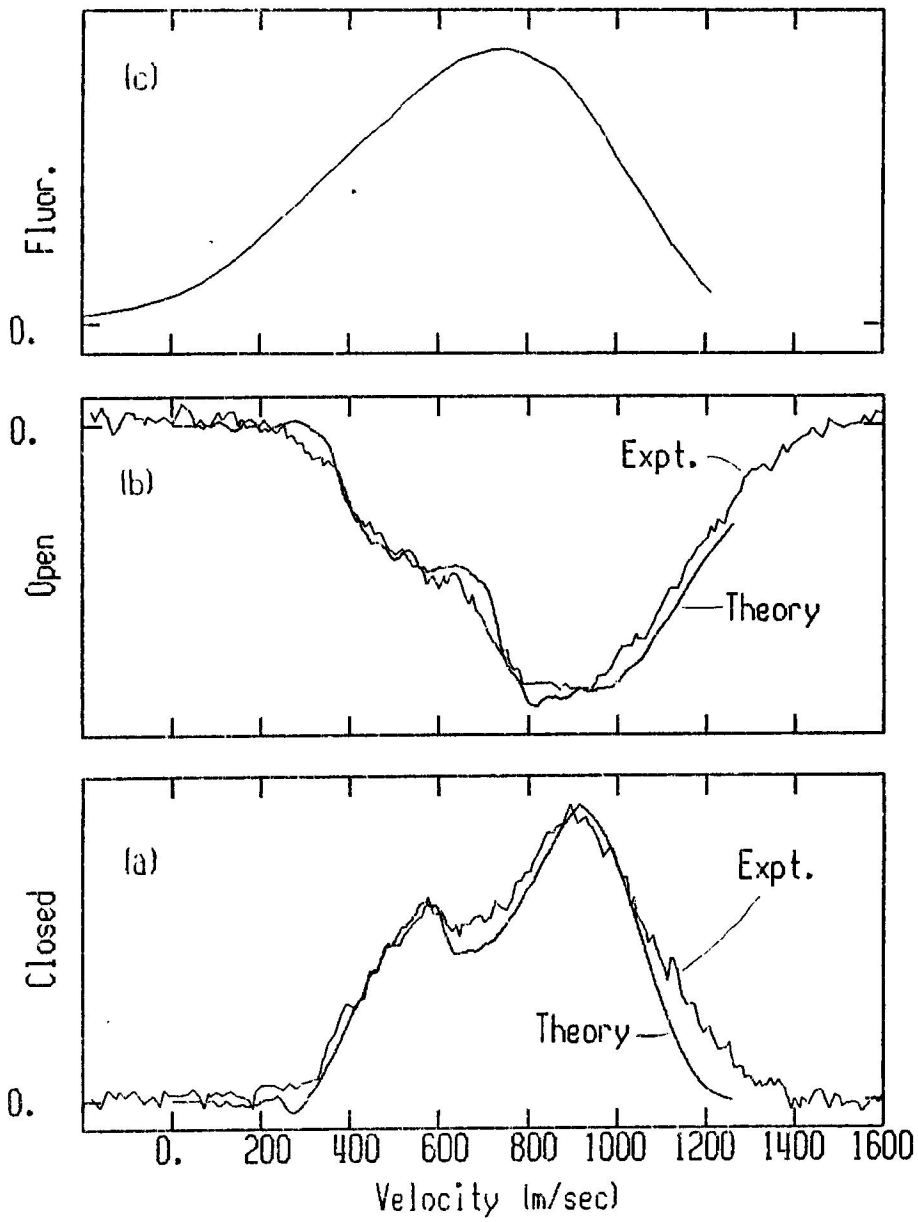

Fig. 8. (a,b) Calculated and observed atomic current as a function laser tuning, in terms of $v_{F=1}$ [via Eq. (1)], for fixed grating relative displacement. (a) AC current at minimum DC current, (b) at maximum DC current. (c) Fluorescence intensity as a function laser tuning, $v_{F=1}$.

filter, whose velocity selectivity allows us to narrow the effective transmitted

velocity range, so as to provide an improvement in the atom-optical spectral resolution. When the gratings are positioned for minimum DC transmission, then neither the laser-ON nor laser-OFF conditions transmit atoms at high velocity. However, the reasons for these two high-velocity cut-offs differ. In the laser-ON condition only low velocity atoms have sufficient scattering angle to reach a G_3 open slit. A cut-off via this process then occurs at an atomic velocity of about 740 m/sec. In the laser-OFF condition only atoms with velocities below $s_2/a_2 \times v_{TR} = 278$ m/sec have sufficiently long de Broglie wavelength so that two adjacent G_2 slits produce overlapping constructive interference at an open G_3 slit. The different cut-off velocities (and profiles) effectively create a "pass-band" that allows resolution of the K^{39} hyperfine structure.

4. HOW DO THESE EXPERIMENTS HELP US TO UNDERSTAND QUANTUM MECHANICS?

They don't! Quantum mechanics is already tough enough to understand. Unfortunately, atom interferometry experiments further exacerbate attempts to form a conceptual model for quantum dynamics. For example, these experiments appear to destroy the conceptual simplicity and elegance of the de Broglie-Bohm guiding-wave model of quantum dynamics and variants thereof discussed at this conference, even beyond the locality problems these models face, *vis à vis* Bell's Theorem. In normal quantum mechanics, the relative magnitudes of an atom's de Broglie wavelength, λ_{dB}, and its so-called "size," $\approx a_0$, are quite unimportant. Indeed, in the experiments of Refs. 6–8, we have $\lambda_{dB} \ll a_0$, in our experiments [4], $\lambda_{dB} \approx a_0$, and in the experiments of Ref. 5, $\lambda_{dB} \gg a_0$. However, via Hamilton-Jacobi theory, in guiding-wave models a particle's translational quantum motion is guided via its "surfing" down a gradient of Bohm's quantum potential. It now becomes difficult to understand just how an atom can so effectively "surf" when its surfboard length ($\approx a_0$) is many times longer than the length of the guiding ripples ($\approx \lambda_{dB}$) in this potential. Even if one describes the wave's propagation in real space as a multi-component vector with components for each constituent part, and also reformulates the quantum potential similarly so that all constituent parts surf together, it remains unclear how one does so and maintains the wholeness of an atom.

Common with everyday experience, one finds no difficuly recognizing that an object may exist (*remain*) at the same position at many different times. These experiments now will force us to think more deeply about the symmetry (and dualism) between space and time. Here, by passing through more than one slit at a time, an atom appears to exist at the same time at many different positions! The English language seems to have no existing

verb that is the space-time dual to *remain.*

ACKNOWLEDGEMENTS

This work was supported by ONR Grant N00014-90-J-1475 and the Firm J. F. Clauser and Associates, Walnut Creek, California. I also acknowledge my thank coworkers S. Li, M. Reinsch, and assistance from G. Garfein, and the staff and students at the UC Berkeley Microstructures Lab.

REFERENCES AND FOOTNOTES

1. S. Altshuler and L. M. Frantz, US Patent # 3,761,721.
2. B. Ya. Dubetskii *et al.*, *Pis'ma, Zh. Eksp. Teor. Fiz.* **39** (11), 531 (1984).
3. J. F. Clauser, *Physica B* **151**, 262 (1988); US Patents # 4,874,942 and # 4,992,656.
4. J. F. Clauser and S. Li, *Phys. Rev. A* **49**, R2213 (1994); *Phys. Rev. A*, Sept. 1994.
5. F. Shimizu *et al.*, *Phys. Rev. A* **46**, R17 (1992); M. Kasevich and S. Chu, *Phys. Rev. Lett.* **67**, 181 (1991).
6. O. Carnal and J. Mlynek, *Phys. Rev. Lett.* **66**, 2689 (1991); F. Riehle *et al.*, *Phys. Rev. Lett.* **67**, 177 (1991).
7. D. W. Keith *et al.* , *Phys. Rev. Lett.* **66**, 2693 (1991).
8. Sterr *et al.*, *Appl. Phys. Lett. B* **54**, 341 (1992).
9. See. J. F. Clauser and A. Shimony, *Rep. Prog. Phys.* **41**, 1881 (1978), and J. F. Clauser, in *Foundations of Quantum Mechanics*, T. D. Black *et al.*, eds. (World Scientific, Singapore, 1992), p. 168.
10. Most quantum mechanics texts don't even display this magic. It can be found, however, in A. Messiah, *Quantum Mechanics* (Wiley, New York, 1962), Vol. II, pp. 395 and 412.
11. S. Li and J. F. Clauser, *Phys. Rev. A* **49**, 2702 (1994).
12. A. Einstein, *Phys. Z.* **18**, 121 (1917), in B. L. van der Waerden, *Sources of Quantum Mechanics* (Dover, New York, 1968), p. 63.
13. O. R. Frisch, *Z. Phys.* **86**, 42 (1933).
14. J. F. Clauser and M. W. Reinsch, *Appl. Phys. B* **54**, 380 (1992), and references therein.
15. D. Walls, *et al.*, in *Foundations of Quantum Mechanics*, T. D. Black *et al.*, eds. (World Scientific, Singapore, 1992), p. 157.
16. Optical pumping is avoided in the cold incident beam experiment above by using a cycling transition, and by applying two laser frequencies for the deflecting light.